

RESEARCH ARTICLE

A new benzimidazole-based selective and sensitive 'on-off' fluorescence chemosensor for Cu²⁺ ions and application in cellular bioimaging

Yi He¹ | Qijing Bing² | Yingjuan Wei¹ | Heyang Zhang² | Guang Wang²¹College of Chemistry, Jilin University, Changchun, P. R. China²Faculty of Chemistry, Northeast Normal University, Changchun, P. R. China**Correspondence**Yi He, College of Chemistry, Jilin University, Changchun 130025, P. R. China.
Email: heyi@jlu.edu.cn**Funding information**

National Natural Science Foundation of China, Grant/Award Number: 50873019

Abstract

Two new twinborn benzimidazole derivatives (**L** and **A**), which bonded pyridine via the ester space on the opposite and adjacent positions of the benzene ring of benzimidazole respectively, were designed and synthesized. Compound **L** displayed fluorescence quenching response only towards copper(II) ions (Cu²⁺) in acetonitrile solution with high selectivity and sensitivity. However, compound **A** presented 'on-off' fluorescence response towards a wide range of metal ions to different degrees and did not have selectivity. Furthermore, compound **L** formed a 1:1 complex with Cu²⁺ and the binding constant between sensor **L** and Cu²⁺ was high at $6.02 \times 10^4 \text{ M}^{-1}$. Job's plot, mass spectra, IR spectra, ¹H-NMR titration and density functional theory (DFT) calculations demonstrated the formation of a 1:1 complex between **L** and Cu²⁺. Chemosensor **L** displayed a low limit of detection ($3.05 \times 10^{-6} \text{ M}$) and fast response time (15 s) to Cu²⁺. The Stern-Volmer analysis illustrated that the fluorescence quenching agreed with the static quenching mode. In addition, the obvious difference of **L** within HepG2 cells in the presence and absence of Cu²⁺ indicated **L** had the recognition capability for Cu²⁺ in living cells.

KEYWORDS

benzimidazole, cell imaging, copper ion, fluorescence chemosensor

1 | INTRODUCTION

Transition metal ions are required and play vital roles in diverse biological processes.^[1] Among them, the copper(II) ion (Cu²⁺) is an essential trace element in biological and fundamental physiological processes, such as a cofactor in a great many enzymes.^[2-5] On the contrary, overloading Cu²⁺ ions in the human body can induce neurodegenerative diseases such as Menkes, Alzheimer and Parkinson.^[6-9] Therefore, the development of new methods to recognize and detect Cu²⁺ ions at lower concentration and with higher sensitivity in the environment and biological systems has become more important.

Up to now, many techniques such as coupled plasma atomic emission spectrometry, atomic absorption spectrometry and electrochemical

method have been used to detect metal ions,^[10-12] but it is difficult for these techniques to execute on-site detection. In recent years, the design and preparation of fluorescent chemosensors to recognize and detect metal ions has attracted increasing interest due to their high selectivity and sensitivity, on-site monitoring, fast response and lower cost.^[13-17] So far, many Cu²⁺ fluorescent chemosensors based on different kinds of materials have been reported.^[18-23]

The benzimidazole moiety as fluorescent material with high fluorescence quantum yield has been used in optical devices^[24-26] and fluorescent chemosensors.^[27,28] However, the reported fluorescence chemosensors with benzimidazole as emitting moiety are not so abundant, therefore development of new benzimidazole-based fluorescent chemosensors to detect Cu²⁺ is still noteworthy.

In this article, two twinborn benzimidazole derivatives (**L** and **A**) with bound pyridine unit via ester space were designed and synthesized (Scheme 1). The difference between these two molecules is the molecular structures, one is a linear molecule (**L**) and the other is a bent-type molecule (**A**). It is hoped that the oxygen atom of the ester space and nitrogen atoms of benzimidazole and pyridine units provide selective coordination points towards metal ions. It was unexpected that the linear compound **L** displayed selective fluorescence quenching response to Cu^{2+} but the bent-type compound **A** indiscriminately responded to most of the tested metal ions to different degrees. Compound **L** displayed not only selective fluorescence response but also the recognition ability to Cu^{2+} ions in living cells. In addition, the sensing mechanism of **L** towards Cu^{2+} ions was also clearly studied.

2 | EXPERIMENTAL

2.1 | Materials and methods

All reagents were of analytical grade from Aladdin Chemical Company and Sinopharm Chemical Reagent Co., Ltd. (Shanghai, China). The mass spectra were recorded on an Agilent mass spectrometer 1200 HPLC/Micro TOF II (Agilent, Santa Clara, USA). $^1\text{H-NMR}$ and $^{13}\text{C-NMR}$ spectra were measured on a Varian Unity Inova Spectrometer (500 MHz and 600 MHz), Varian, Walnut Creek, CA, USA, using deuterated chloroform (CDCl_3) and dimethyl sulfoxide ($\text{DMSO-}d_6$) as solvents. Fluorescence spectra and absorbance spectra were tested on a Varian Cary Eclipse fluorescence spectrophotometer (Varian, Walnut Creek, CA, USA) and Varian Cary 500 UV-visible spectrophotometer (Varian, Walnut Creek, CA, USA), respectively. Fluorescence microscope images were taken on an Olympus FV-1000 Confocal Laser Scanning Microscope (Olympus, Tokyo, Japan). A METTLER FE20 pH meter was used to measure pH values of solutions (Mettler-Toledo, Zurich, Suisse). The stock solutions of all tested metal ions were prepared using the following salts: AgNO_3 , $\text{Zn}(\text{NO}_3)_2 \cdot 6\text{H}_2\text{O}$, KNO_3 , $\text{Cd}(\text{NO}_3)_2 \cdot 4\text{H}_2\text{O}$, $\text{Ni}(\text{NO}_3)_2 \cdot 6\text{H}_2\text{O}$, $\text{Cu}(\text{NO}_3)_2 \cdot 3\text{H}_2\text{O}$, $\text{Cr}(\text{NO}_3)_3 \cdot 9\text{H}_2\text{O}$, $\text{Al}(\text{NO}_3)_3 \cdot 9\text{H}_2\text{O}$, $\text{Fe}(\text{NO}_3)_3 \cdot 9\text{H}_2\text{O}$, $\text{Mg}(\text{NO}_3)_2 \cdot 6\text{H}_2\text{O}$, $\text{BaCl}_2 \cdot 2\text{H}_2\text{O}$, $\text{Co}(\text{NO}_3)_2 \cdot 6\text{H}_2\text{O}$, MnCl_2 , SrSO_4 , CaCl_2 , PbCl_2 , HgCl_2 and $\text{FeSO}_4 \cdot 7\text{H}_2\text{O}$.

2.2 | Synthesis

2.2.1 | Synthesis of precursors 4-(1H-benzo[d]imidazol-2-yl)phenol (compound 1) and 4-(1H-benzo[d]imidazol-2-yl)phenol (compound 2)

Compounds **1** and **2** were synthesized using the following procedure:

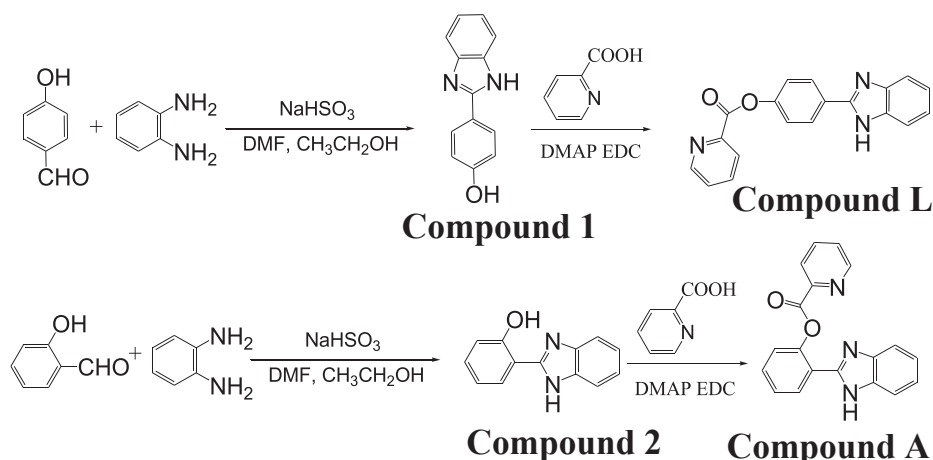
Compound **1** – *p*-hydroxy benzaldehyde (3.05 g, 25 mmol) and sodium hydrogen sulfate (5.20 g, 50 mmol) were dissolved in 20 mL anhydrous ethanol ($\text{C}_2\text{H}_5\text{OH}$) in a flask, the reaction mixture was stirred at room temperature for 6 h. Then 20 mL *N,N*-dimethylformamide and *o*-phenylenediamine (5.40 g, 50 mmol) were added into the reaction mixture. After the mixture was heated at reflux temperature for 4.5 h, it was cooled down to room temperature and poured into 300 mL distilled water. The precipitate was collected and recrystallized in anhydrous $\text{C}_2\text{H}_5\text{OH}$, faint yellow solid powder was obtained, 8.34 g, yield 89.7%. $^1\text{H-NMR}$ (600 MHz, DMSO) δ 12.72 (s, 1H), 8.10 (d, *J* 8.7 Hz, 2H), 7.61 (d, *J* 7.5 Hz, 1H), 7.49 (d, *J* 7.4 Hz, 1H), 7.19–7.09 (m, 4H), 4.91 (t, *J* 5.5 Hz, 1H).

Compound **2** – yield, 80.8%. $^1\text{H-NMR}$ (600 MHz, CDCl_3) δ 13.07 (s, 1H), 9.35 (s, 1H), 7.80–7.75 (m, 1H), 7.58 (dd, *J* 7.8, 1.5 Hz, 1H), 7.51 (dd, *J* 5.6, 3.1 Hz, 1H), 7.38 (ddd, *J* 8.5, 7.3, 1.6 Hz, 1H), 7.34–7.30 (m, 2H), 7.14 (dd, *J* 8.3, 0.9 Hz, 1H), 6.99–6.95 (m, 1H).

2.2.2 | Synthesis of compounds L and A

Compound **L** (4-(1H-benzo[d]imidazol-2-yl)phenyl picolinate) and compound **A** (2-(1H-benzo[d]imidazol-2-yl)phenyl picolinate) were prepared also using the same procedure:

Compound **L** – picolinic acid (0.74 g, 6 mmol), compound **1** (1.89 g, 6 mmol) and 4-dimethylaminopyridine (DMAP, 0.15 g, 1.25 mmol) were added into 40 mL purified dichloromethane in 100 mL flask, the mixture was stirred for 1 h at room temperature. After 1-ethyl-3-(3-dimethylaminopropyl)carbodiimide hydrochloride (EDC, 1.44 g, 7.5 mmol) was added, the resultant mixture was continuously stirred under nitrogen gas for 24 h. The organic phase was



SCHEME 1 Synthesis of compounds **L** and **A**

washed with distilled water and then approximately 25 mL of dichloromethane was evaporated under vacuum. The white product was obtained by filtration, 1.37 g, yield 72.6%. $^1\text{H-NMR}$ (600 MHz, DMSO) δ 12.99 (s, 1H), 8.85 (d, J 4.0 Hz, 1H), 8.32–8.23 (m, 3H), 8.12 (td, J 7.7, 1.7 Hz, 1H), 7.77 (ddd, J 7.7, 4.7, 1.0 Hz, 1H), 7.62 (s, 2H), 7.53 (d, J 8.7 Hz, 2H), 7.23 (dd, J 5.8, 3.0 Hz, 2H), 5.75 (s, 1H). $^{13}\text{C-NMR}$ (151 MHz, DMSO) δ 163.81, 152.27, 151.02, 150.56, 147.13, 138.28, 128.64, 128.56, 128.30, 126.29, 122.97, 55.38, 40.41, 40.28, 40.17, 40.14, 40.00, 39.86, 39.73, 39.72, 39.58. HRMS: m/z : found $[\text{M} + \text{Na}^+]$ 338.0913, molecular formula $\text{C}_{19}\text{H}_{13}\text{N}_3\text{O}_2$, requires $[\text{M} + \text{Na}^+]$ 338.3140.

Compound **A** – yield 68.5%. $^1\text{H-NMR}$ (600 MHz, CDCl_3) δ 13.25 (s, 1H), 9.12–9.01 (m, 1H), 8.80 (dd, J 7.9, 1.7 Hz, 1H), 8.36 (d, J 7.8 Hz, 1H), 8.06 (td, J 7.7, 1.7 Hz, 1H), 7.99 (dd, J 8.3, 1.0 Hz, 1H), 7.85 (dd, J 5.6, 2.9 Hz, 1H), 7.75 (ddd, J 7.6, 4.8, 1.1 Hz, 1H), 7.58 (dd, J 5.7, 3.0 Hz, 1H), 7.52 (ddd, J 8.3, 7.4, 1.8 Hz, 1H), 7.47–7.41 (m, 1H), 7.32–7.27 (m, 2H). $^{13}\text{C-NMR}$ (151 MHz, CDCl_3) δ 161.40, 149.07, 148.39, 148.20, 147.15, 138.21, 130.31, 128.28, 126.29, 122.97, 122.33, 121.48, 119.55, 111.04, 77.25, 77.04, 76.83. HRMS: m/z : found $[\text{M} + \text{H}^+]$ 316.1089, molecular formula $\text{C}_{19}\text{H}_{14}\text{N}_3\text{O}_2$, requires $[\text{M} + \text{H}^+]$ 316.3320.

2.3 | Preparation of stock solutions

The stock solutions of compounds **L** and **A** were prepared with the concentration of 1×10^{-4} M in different solvents including acetonitrile (CH_3CN), $\text{C}_2\text{H}_5\text{OH}$, $\text{CH}_3\text{CN-Tris}$ (20 mM, pH 7.2, 1:1 v/v), $\text{C}_2\text{H}_5\text{OH-Tris}$ (20 mM, pH 7.2, 1:1 v/v).

The stock solutions of different metal ions (5 mM) in distilled water were made of their inorganic salts: chloride salts (Cu^{2+} , Co^{2+} , Ni^{2+} , Ba^{2+} , Hg^{2+} , Mn^{2+} , Pb^{2+} , Ca^{2+}), nitrate salts (Al^{3+} , Zn^{2+} , Fe^{3+} , Cr^{3+} , K^+ , Mg^{2+} , Cd^{2+} and Ag^+), and sulfate salts (Sr^{2+} and Fe^{2+}).

3 | RESULTS AND DISCUSSION

3.1 | Synthesis and characterization

The synthetic routes are shown in scheme 1. Compounds **A** and **L** were synthesized by the esterification reaction of picolinic acid and phenolic hydroxyl group of benzimidazole compounds with high yield

under the catalytic effect of DMAP and EDC. The structure of compounds **L** and **A** were well characterized by high-resolution mass spectrometry (HRMS), $^1\text{H-NMR}$, and $^{13}\text{C-NMR}$ analyses (Figures S1–S8). It is hoped that the oxygen atom of the ester group and the nitrogen atoms of benzimidazole and pyridine play a synergistic effect to coordinate with special metal ions. The linear and non-linear molecular structures present different steric configurations and are expected to display different coordination selectivity towards metal ions.

3.2 | Absorption and fluorescence spectra of compounds **L** and **A** and their response towards metal ions

The fluorescence and absorbance spectra of compounds **L** and **A** (10 μM) in CH_3CN solutions are presented in Figure 1(a). The main absorbance bands of **L** and **A** are located at 296 nm, which can be ascribed to π - π^* electron transition within their whole molecules.^[17,18] In the same solutions, compounds **L** and **A** displayed strong fluorescence emissions. Compound **L** presented two emission peaks at 341 nm and 356 nm, respectively. Compound **A** just presented one emission band at 461 nm and a large red-shift compared with that of **L**, which may be due to the larger π conjugation system in molecule **A** than **L**.

Selectivity is the first consideration for a chemosensor to be suitable in practical applications, so the absorbance and fluorescence response towards different metal ions were the primary investigations in the different solvent systems as follows, CH_3CN , $\text{C}_2\text{H}_5\text{OH}$, $\text{CH}_3\text{CN-Tris}$ (20 mM, pH 7.2, 1:1 v/v), $\text{C}_2\text{H}_5\text{OH-Tris}$ (20 mM, pH 7.2, 1:1 v/v). After the addition of a different metal ion (5 equivalents) to **L** or **A** solution (10 μM) and mixing for 15 s, the UV-visible absorbance and fluorescence spectra were measured at room temperature. For measurements of fluorescence spectra, the light of 305 and 330 nm was used as excitation wavelength for compounds **L** and **A**, respectively. In the solvent systems of $\text{C}_2\text{H}_5\text{OH}$, $\text{CH}_3\text{CN-Tris}$ (20 mM, pH 7.2, 1:1 v/v) and $\text{C}_2\text{H}_5\text{OH-Tris}$ (20 mM, pH 7.2, 1:1 v/v), all the absorbance and fluorescence of compounds **L** and **A** displayed responses to most of the test metal ions but the responses were to different degrees and there was no regularity. These results indicated that most test metal ions affected the photophysical properties of compounds **L** and **A**. Therefore, in these three solvent systems,

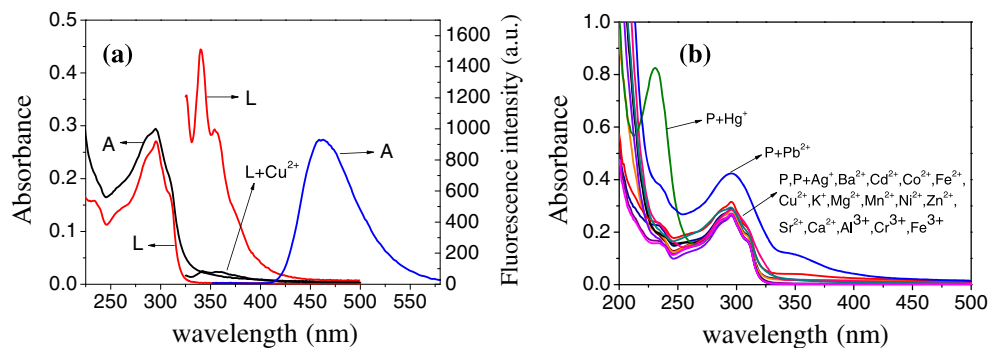


FIGURE 1 (a) The absorbance and fluorescence spectra of compounds **L** and **A** in acetonitrile (CH_3CN) solutions (10 μM) and fluorescence spectrum of **L** in CH_3CN solution (10 μM) upon the addition of Cu^{2+} ions (5 equivalents of **L**). $\lambda_{\text{ex}} = 305$ nm for **L** and $\lambda_{\text{ex}} = 330$ nm for **A**. (b) The absorbance changes of compound **L** in CH_3CN solutions (10 μM) upon the addition of 5 equivalents of different metal ions

compounds **L** and **A** were not suitable to be used as chemosensors of metal ions.

However, compound **L** displayed selective fluorescence response to Cu^{2+} ions in pure CH_3CN solution, only the addition of Cu^{2+} caused significant fluorescence quenching of compound **L** (Figure 1a). The absorbance spectra and colors of **L** in CH_3CN did not change noticeably after the addition of the test metal ions (Figure 1b) indicating **L** could not be used as a colorimetric chemosensor for metal ions. The absorbance spectra changes of **L** induced by Hg^{2+} and Pb^{2+} were ascribed to the interaction between Hg^{2+} and Pb^{2+} ions with CH_3CN molecules.^[16,18] On the contrary, the absorbance and fluorescence spectra of compound **A** in CH_3CN solution did not show selective responses towards metal ions (Figure S9), which indicated that compound **A** could not be used as a chemosensor for metal ions.

The results of the photophysical investigation on compounds **L** and **A** indicated that only **L** was suitable for fluorescence sensing of Cu^{2+} ions in CH_3CN solution.

3.3 | Fluorescence sensing of compound **L** towards Cu^{2+} ions

The earlier primary photophysical investigation of compound **L** towards metal ions showed that **L** can be used as a selective fluorescence chemosensor for Cu^{2+} . In order to further confirm this conclusion, the selectivity of **L** towards different metal ions was then investigated in detail. After the additions of different metal ions (5 equivalents of **L**) into solutions of compound **L** (10 μM) in CH_3CN respectively, the metal ions such as K^+ , Ag^+ , Cd^{2+} , Co^{2+} , Mg^{2+} , Hg^{2+} , Ni^{2+} , Mn^{2+} , Ba^{2+} , Pb^{2+} , Ca^{2+} , Na^+ and Fe^{2+} did not impact any influence on the fluorescence spectra. Furthermore, Cr^{3+} , Al^{3+} , Fe^{3+} ions did not show any obvious influence on the fluorescence intensity of **L** at 356 nm but quenched the emission band at 340 nm and shifted emission to red. The Zn^{2+} was a special case, it made the fluorescence spectrum of compound **L** increase and red-shift, which could be ascribed to the formation of a complex between **L** and Zn^{2+} ion to a small extent. Only Cu^{2+} markedly impacted on the whole fluorescence

spectra of **L** and largely quenched fluorescence intensity (Figure 2a). The fluorescence intensity of **L** at 340 and 356 nm was quenched by 95.0% and 92.6% respectively upon the addition of 5.0 equivalents of Cu^{2+} , the fluorescence was changed from 'on' to 'off'. The fluorescence photographs of **L** in CH_3CN solution in the absence and presence of Cu^{2+} ions further illustrated the quenching effect of Cu^{2+} ion on the emission of **L** in Figure 2(b). This result indicated the excellent fluorescence selectivity of **L** towards Cu^{2+} ion in CH_3CN solution. Although the additions of Cr^{3+} , Al^{3+} and Fe^{3+} ions caused changes of the emission band at 340 nm, they gave very little influence on the fluorescence intensity at 356 nm. Therefore, monitoring fluorescence intensity at 356 nm of **L** can recognize and quantify Cu^{2+} ions. Furthermore, the reason for the fluorescence quenching was possibly owing to formation of the complex $\text{L}-\text{Cu}^{2+}$ and then the paramagnetic characteristic of Cu^{2+} caused the fluorescence quenching. The electrons of the excited states of benzimidazole can transfer to the unpaired d-orbital of copper ions and further quench the fluorescence of **L**.^[29-33] The results demonstrated that **L** can recognize Cu^{2+} with high selectivity in pure CH_3CN solution.

The reversible fluorescence response can further explain the formation of the complex $\text{L}-\text{Cu}^{2+}$. A solution of compound **L** (10 μM) containing Cu^{2+} (2 equivalents of **L**) in CH_3CN was added to an excess of ethylenediamine tetraacetic acid (EDTA, 4 equivalents of **L**), the fluorescence spectrum obtained was nearly restored to the original spectrum of **L** solution (Figure S10). This result indicated that the fluorescence quenching of **L** by Cu^{2+} was due to the reversible complex formation process.

Job's plot is often used to evaluate complex ratio. In the series of CH_3CN solutions, the constant concentration of **L** and Cu^{2+} in each solution was 50 μM and the molar ratios of **L** and Cu^{2+} ion were variable. The emission intensity at 340 nm was plotted against the fraction of **L**. The maximum appeared at 0.5 molar fraction of **L** indicating a 1:1 complex ratio between **L** and Cu^{2+} . The 1:1 complex ratio was further proved by electrospray ionization (ESI)-HRMS spectra. To prepare the mass spectrum sample, the excess solid $\text{Cu}(\text{NO}_3)_2 \cdot 3\text{H}_2\text{O}$ was added into the solution of **L** in $\text{DMSO}-d_6$. After a sufficient reaction time, the liquid supernatant was used to measure

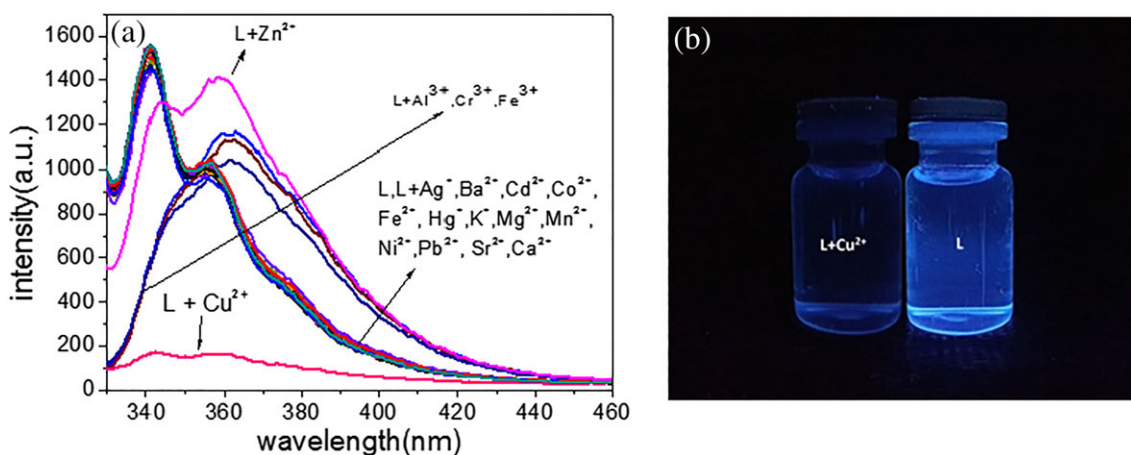


FIGURE 2 (a) Fluorescence response of compound **L** (10 μM) in acetonitrile (CH_3CN) to different metal ions (5.0 equivalents of **L**). (b) Fluorescence photographs of compound **L** in the absence and presence of 5 equivalents of Cu^{2+} . (For an interpretation of the reference to the color in this figure, the readers are referred to the website version of this article.)

the mass spectrum. As shown in Figure S11, a molecular-ion peak at $m/z = 400.2713$ belonged to $[L + Cu^{2+} + H_2O + 4H^+]^+$ species (calculated 400.6945). Another molecular-ion peak at $m/z 458.2369$ corresponded to the complex of $[L + Cu^{2+} + CH_3CN + Cl^- + 3H^+]^+$ (calculated 458.1745). The results of the mass spectra also indicated that both Cl^- ion and H_2O molecule took part in the coordination reaction of **L** with Cu^{2+} . To further confirm the 1:1 complex ratio and investigate the role of the counter anion in the coordination process, the complex reaction of **L** with $Cu(NO_3)_2$ was carried out. The mass spectrum of the complex sample was also measured and shown in Figure S12. As the previous mass spectrum, the molecular-ion peak at $m/z = 400.2638$ ascribed to $[L + Cu^{2+} + H_2O + 4H^+]^+$ species also appeared. Another different molecular-ion peak at $m/z 457.2557$ corresponded to the complex of $[L + Cu^{2+} + CH_3CN + 2H_2O + 2H^+]^+$ (calculated 457.1037). The two peaks further demonstrated the 1:1 complex ratio between **L** and Cu^{2+} . The molecular-ion peak corresponded to NO_3^- -containing complex was not found, which indicated that the counter anion NO_3^- did not take part in the complex reaction.

Fast fluorescence response of a chemosensor is more suitable for on-site monitoring in practical applications. The fluorescence at 340 nm of **L** solution was monitored and rapidly decreased to equilibrium point within 15 s after addition of Cu^{2+} ions (Figure S13), which indicated that **L** had the capability for on-site monitoring.

High capacity of resisting interference is more beneficial to chemosensors in practical applications and can be testified via the following experiment. The possible interference of other metal ions including Fe^{3+} , Ag^+ , K^+ , Al^{3+} , Cr^{3+} , Mg^{2+} , Cd^{2+} , Co^{2+} , Hg^{2+} , Zn^{2+} , Ni^{2+} , Mn^{2+} , Ca^{2+} , Ba^{2+} , Pb^{2+} , Sr^{2+} and Fe^{2+} were taken into consideration for a chemosensor in a practical application. After the addition of 5 equivalents of other metal ions to the solutions of **L** (10 μ M) containing 5 equivalents of Cu^{2+} in CH_3CN respectively, their fluorescence intensities at 356 nm were measured and the results are shown in Figure 3(b). In all the tested solutions, the addition of Cu^{2+} ions caused fluorescence quenching near to that of the **L** solution only containing Cu^{2+} ions. The experiment proved that compound **L** can recognize Cu^{2+} over a variety of coexisting metal ions.

The sensing property of **L** for Cu^{2+} ions was studied using fluorescence titration. The fluorescence emission titration experiments of **L** (10 μ M) with Cu^{2+} (0–5 equivalents) in CH_3CN were carried out

(Figure 4a), the Cu^{2+} solution in water was incrementally added into **L** solution in CH_3CN (10 μ M). The added maximal volume of Cu^{2+} solution was smaller than 2% volume of **L** solution to avoid the large change of the concentration of **L**. The fluorescence intensity of **L** at 356 nm was gradually quenched with the incremental Cu^{2+} concentration (Figure S14). When the concentration of Cu^{2+} reached about 3.5 equivalents of **L**, the fluorescence of sensor **1** decreased to the equilibrium value and all the fluorescence was almost quenched. The curve of the fluorescence intensity at 356 nm as a function of Cu^{2+} concentration in the range 2–17 μ M was a straight line with a large correlation coefficient of $R^2 = 0.99362$. From this calibration curve, the limit of detection (LOD) was calculated to be 3.05×10^{-6} mol/L according to the equation of $(3\sigma/K)$.^[34] This LOD was lower than the standard value of copper in drinking water (~20 μ M) specified by the US Environment Agency.^[35] The LOD and linearity range provided evidence that **L** was suitable for quantitative determination of Cu^{2+} concentration in water samples.

The affinity of **L** with Cu^{2+} could be evaluated according to the value of the binding constant (K_a) of the **L**– Cu^{2+} complex, which can be calculated from the Benesi–Hildebrand (B-H) plot based on the following equation:^[36]

$$1/(F_0 - F) = 1/\{K_a(F_0 - F_{min})C\} + 1/(F_0 - F_{min})$$

where C is the concentration of Cu^{2+} solution, F_0 was the fluorescence intensity of **L** at 356 nm without Cu^{2+} and F was the fluorescence intensity upon the addition of different concentrations of Cu^{2+} . Thus, F_{min} is the minimum value of the fluorescence intensity upon the addition of excess Cu^{2+} ions. The experimental curve was fitted according to the 1:1 complex ratio and the fitting curve was almost a linear relationship with a high correlation coefficient of 0.99152 (Figure 4b), which also confirmed the 1:1 complex ratio between **L** with Cu^{2+} . The K_a value was calculated to be $6.02 \times 10^4 M^{-1}$ from the intercept and slope of the linear fitting plot indicating strong affinity of **L** with Cu^{2+} .

3.4 | Study on the fluorescence quenching mechanism

Generally, there are two quenching mechanisms above fluorescence quenching, static and dynamic quenching. Stern–Volmer curves are

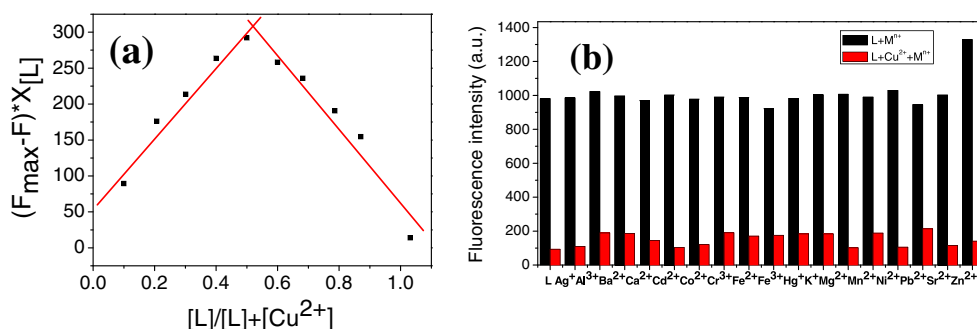


FIGURE 3 (a) Job's plot from the fluorescence intensity at 340 nm of **L** and Cu^{2+} in acetonitrile (CH_3CN) solution with a total concentration of 50 μ M ($\lambda_{ex} = 305$ nm). (b) The fluorescence intensity changes at 356 nm of **L** (10 μ M) in CH_3CN solutions upon the addition of different metal ions. The black bars represent the fluorescence intensity of **L** at 356 nm after the addition of different metal ions (5 equivalents of **L**), the red bars represent the fluorescence intensity of the earlier solutions after a further addition of 5 equivalents of Cu^{2+} , respectively

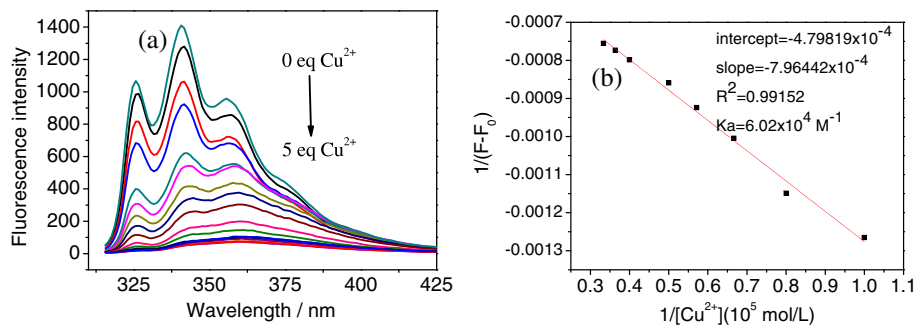


FIGURE 4 (a) The changes of fluorescence spectra of **L** (10 μM) in acetonitrile (CH_3CN) solution with incremental addition of Cu^{2+} (0–5 equivalents of **L**). (b) The Benesi–Hildebrand plot of the titration experiment of **L** with Cu^{2+} ions in CH_3CN solution

often used to investigate the nature of the quenching mechanism in the complexing process. Two different forms of fluorescence intensities ($\ln F_0/F$ or F_0/F) were plotted as a function of Cu^{2+} concentration, in which, the linear curve belongs to the true quenching mode.^[37]

$$\ln \frac{F_0}{F} = e^{K_{sv}[M]} \text{ Static quenching}$$

$$\frac{F_0}{F} = 1 + K_{sv}[M] \text{ Dynamic quenching}$$

where F and F_0 are the fluorescence intensities of **L** at 356 nm in the presence and absence of Cu^{2+} , respectively, $[M]$ is the concentration of Cu^{2+} and K_{sv} is the Stern–Volmer quenching constant. As shown in Figure 5, F_0/F (black line) did not show a linear relationship with Cu^{2+} concentration, which suggested the fluorescence quenching did not belong to dynamic quenching. On the contrary, the plot of $\ln F_0/F$ values against Cu^{2+} concentrations was a linear curve; the fitting curve with a high correlation coefficient ($R^2 = 0.99521$) was superimposed together with the experimental plot. This result illustrated that the fluorescence quenching process was concurrent with the Perrin model of static quenching (blue line) and proves that fluorescence quenching occurs intramolecularly in the **L**- Cu^{2+} complex.

3.5 | Possible sensing mechanism

Aforementioned results of photophysical studies and mass spectra suggested that the sensing response of **L** towards Cu^{2+} was ascribed to the formation of 1:1 **L**- Cu^{2+} complexes. To further prove the

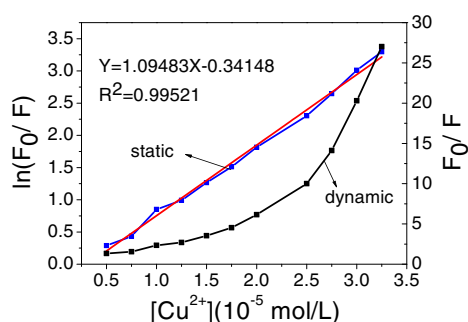


FIGURE 5 Stern–Volmer quenching analysis plots of **L** upon the addition Cu^{2+}

1:1 **L**- Cu^{2+} complex formation, the density functional theory (DFT) calculations, $^1\text{H-NMR}$ titration and IR spectra were carried out.

The DFT calculation was completed using the *B3LYP/6-31G(d)* level of Gaussian 09 package to further study the interaction mechanism between **L** and Cu^{2+} .^[38] The optimized ground-state geometries of the complex showed a 1:1 binding stoichiometry in Figure 6(a). Compound **L** provided two coordination sites, the nitrogen atom of pyridine and the oxygen atom of the carbonyl via lone-pair electrons.

The frontier orbital energies and shapes were presented in Figure 6(b), the main highest occupied molecular orbital (HOMO) and the lowest unoccupied molecular orbital (LUMO) of **L** were centered on the benzimidazole moiety and pyridine ring. On the contrary, all the HOMO and LUMO of the **L**- Cu^{2+} complex were localized in the pyridine part indicating the existence of a charge transfer from benzimidazole to Cu^{2+} and further causing the fluorescence quenching. The energy gap between the LUMO and HOMO of **L**- Cu^{2+} was calculated to be 0.33 eV and was much smaller than that of **L** (3.82 eV), which indicated the formation of a stable complex. The HOMO energy (-12.69 eV) of **L**- Cu^{2+} complex was very much smaller than that of **L** (-6.06 eV) indicating electrons on the HOMO of the complex was more stable and had lower reactive activity.^[39,40] In addition, the absorbance spectrum of **L** was also optimized by DFT calculations under the consideration of the solvent effect, Figure S15. The optimized maximum absorbance band was at 298 nm, which was very close to the experimental value (296 nm) and also indicated that the DFT calculation results were in very good agreement with the experimental results. The earlier results confirmed the 1:1 stoichiometry of the **L**- Cu^{2+} complex and indicated that the nitrogen atom of pyridine and oxygen atom of carbonyl coordinated with Cu^{2+} .

$^1\text{H-NMR}$ titration in $\text{DMSO-}d_6$ also provided obvious proof of coordination interaction between **L** and Cu^{2+} , the results are shown in Figure S16. The changes of the integral area and position of hydrogen peaks illustrated the coordination interaction between **L** and Cu^{2+} . The peak at 8.80 was ascribed to the hydrogen adjacent to the nitrogen atom of the pyridine unit and vanished completely after the addition of 0.5 equivalents Cu^{2+} of **L**, which indicated the participation of the nitrogen atom of pyridine in the coordination of **L** with Cu^{2+} . On the contrary, the peak at 5.75 corresponding to the hydrogen of imine of benzimidazole decreased gradually with Cu^{2+} increasing but did not shift or vanish, which showed that the nitrogen atom of amine did not take part in the coordination process. The other proton peaks

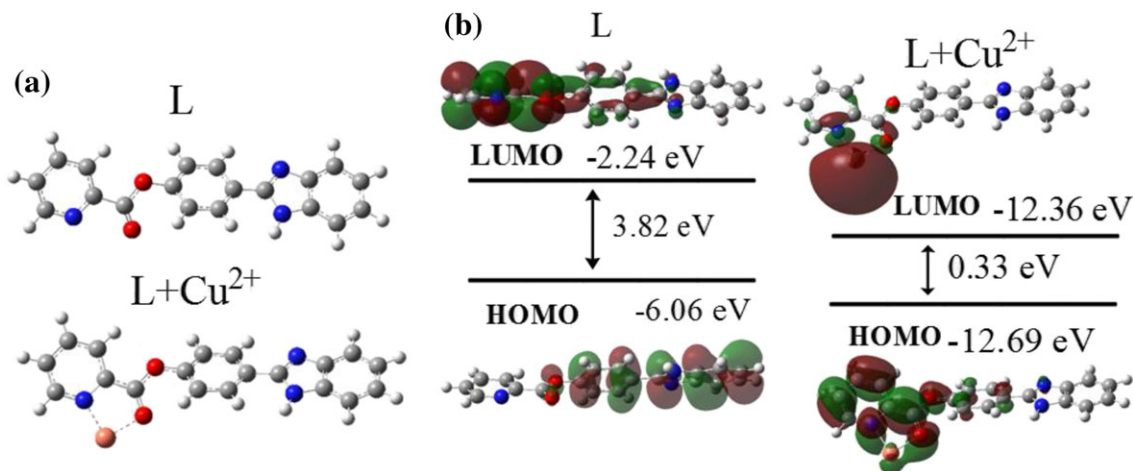


FIGURE 6 (a) Optimized ground-state geometries and orbital energy level of L and L-Cu²⁺. Color code: C (gray), O (red), N (blue), H (white), Cu²⁺ (orange). (b) LUMO and HOMO orbital shapes of L-Cu²⁺ complex and L. (For interpretation of the reference to color in this figure legend, the readers are referred to the website version of this article.)

gradually decreased with the increment of Cu²⁺ ions accompanied with the high-field shift. These results clearly revealed the occurrence of a complex reaction between L with Cu²⁺ and the nitrogen atoms on pyridine were the coordination sites for Cu²⁺.

Infrared (IR) spectra results also provided the evidence of the coordination interaction of L with Cu²⁺. The complex L-Cu²⁺ sample for IR spectrum was prepared as for the samples for HRMS spectra. The absorption peak of carbonyl of ester of L appeared at 1754 cm⁻¹, the broad absorption peak at 3424 cm⁻¹ was caused by the formation of hydrogen-bond due to the existence of oxygen and nitrogen atoms (Figure S17). After the formation of the complex, the carbonyl absorption peak disappeared indicating the participation of the carbonyl group in the coordination process with Cu²⁺. Meanwhile, the peak of the stretching vibration of benzene skeleton was extruded and presented a very strong peak at 1600 cm⁻¹. On the contrary, the amine peak at 3424 cm⁻¹ did not vanish, which demonstrated that the nitrogen atom

of the imino group did not take part in the coordination reaction. In addition, most of the peaks in the fingerprint region vanished upon the coordination effect. These results indicated that the nitrogen atom of pyridine and the oxygen atom of the carbonyl groups of L were coordination points for Cu²⁺.

Based on the earlier evidence, the proposed binding mode of L with Cu²⁺ and the fluorescence quenching mechanism are shown in Scheme 2.

4 | ANALYTICAL APPLICATIONS

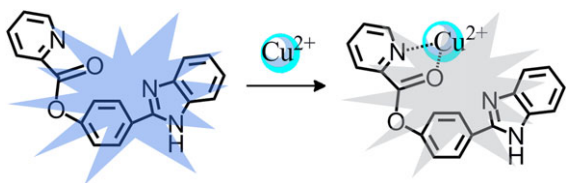
From the earlier experimental results, L can recognize and detect Cu²⁺ in water samples. To prove this result, the recovery experiment of water samples and fluorescent images in living cells were executed.

4.1 | Recovery experiments in water samples

The drinking and tap water samples were used in Cu²⁺ recovery experiments, each sample was measured with four replicates and the results are shown in Table 1. The recovery and relative standard deviation (RSD) values of four samples were satisfactory. The recovery results proved that sensor L could be useful in the quantitative detection of Cu²⁺ in environmental water samples.

4.2 | Fluorescence bioimaging for living cells

The high selective and sensitive fluorescence response of L towards Cu²⁺ ions encouraged us to study the possibility of Cu²⁺ recognition in living cells via the cell imaging experiments. The liver cancer HepG2 cells were chosen for the fluorescence imaging experiments. First, we prepared a solution (20 μM) of L in DMSO and a solution of Cu²⁺ (40 μM) in empty medium. Then well 1 and 2 were loaded with 500 μL cell suspension, respectively. Then, well 1 was added with 10 μL Cu²⁺ solution and incubated at 37°C for 30 min and then washed twice with phosphate-buffered saline (PBS) solution. After



SCHEME 2 The proposed binding mode of L with Cu²⁺ and its fluorescence quenching mechanism

TABLE 1 The analytical results of copper(II) ion (Cu²⁺) in water samples (n = 4)^a

Samples	Added (μM)	Found ^b (μM)	Recovery (%)	RSD ^c (%)
Tap water	4.0	4.08	102.0	0.21
	8.0	8.08	100.75	0.43
Drinking water	4.0	3.96	99.0	0.31
	8.0	7.99	99.88	0.29

^aConditions: [Sensor L] = 10 μM in acetonitrile solution. ^bMean values of four determinations. ^cRelative standard deviation of four determinations.

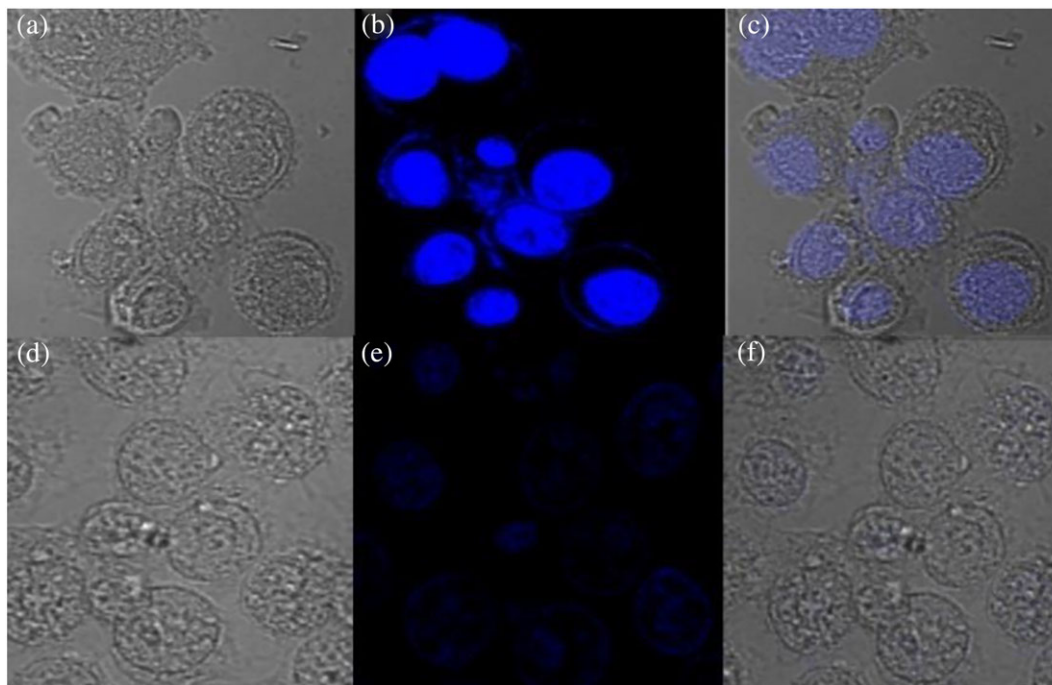


FIGURE 7 Confocal fluorescence images of living HepG2 cells. (a) Bright field image of the HepG2 cells only pre-incubated with L. (b) Fluorescence image of (a). (c) Overlay image of (a) and (b). (d) Bright field image of HepG2 cells pre-incubated with Cu^{2+} for 30 min and then incubated with L. (e) Fluorescence image of (d). (f) Overlay image of (d) and (e)

that, wells 1 and 2 were added with 10 μL L solution respectively and incubated for 90 min. After being washed twice with PBS solution, the two kinds of treated cells were placed on glass slides for fluorescence imaging.

As shown in Figure 7, the cells only incubated with L showed a strong fluorescence (Figure 7b), whereas the cells incubated with both Cu^{2+} and L displayed obvious fluorescence quenching (Figure 7e) indicating obvious fluorescence quenching effect of Cu^{2+} ions on L in living cells. This result confirmed that L can coordinate with Cu^{2+} ions and recognize Cu^{2+} ions in living cells.

5 | CONCLUSIONS

Two new pyridine-containing twinborn benzimidazole derivatives (L and A) were designed and synthesized. Only L displayed highly selective and sensitive sensing for Cu^{2+} via fluorescence quenching. The fluorescent intensity of L presented a linear relationship with Cu^{2+} in the concentration range 2–17 μM and the LOD of L for Cu^{2+} was calculated to be 3.05×10^{-6} M. The results of Job's plot, mass spectra, IR spectra, $^1\text{H-NMR}$ titration and DFT calculation revealed that the fluorescence quenching was caused by the formation of a 1:1 L– Cu^{2+} complex. A Stern–Volmer investigation indicated that the fluorescence quenching met the static quenching. Compound L displayed great potential for applications in the detection of Cu^{2+} ions in water samples and recognition of Cu^{2+} ions in living cell via fluorescence imaging.

ACKNOWLEDGEMENT

The authors are grateful for financial support from the National Natural Science Foundation of China (no. 50873019).

ORCID

Yi He  <https://orcid.org/0000-0002-2616-0497>

REFERENCES

- [1] P. C. Kyle, M. Y. Alexandra, E. P. Amy, *Chem. Rev.* **2014**, *114*, 4564.
- [2] R. Uauy, M. Olivares, M. Gonzalez, *Am. J. Clin. Nutr.* **1998**, *952s*, 67.
- [3] K. J. Barnham, C. L. Masters, A. I. Bush, *Nat. Rev. Drug. Discov.* **2004**, *3*, 205.
- [4] S. Arjunan, S. Gopalan, S. Selvaraj, S. Thangaraj, M. P. Subramaniam, *J. Photoch. Photobio. A* **2018**, *364*, 424.
- [5] W. J. Xu, D. Q. Qi, J. Z. You, F. F. Hu, J. Huang, *J. Mol. Struct.* **2015**, *1091*, 133.
- [6] D. J. Ghosh, S. Rhodes, D. Winder, A. Atkinson, K. Aiken, *J. Mol. Struct.* **2017**, *1134*, 638.
- [7] Y. Shiono, H. Hayashi, S. Wakusawa, M. Yano, *Med. Electron. Microsc.* **2001**, *34*, 54.
- [8] P. G. Georgopoulos, A. Roy, M. J. Yonone-Lioy, R. E. Opiekun, P. J. Lioy, *J. Toxicol. Environ. Health. B* **2001**, *4*, 341.
- [9] D. J. Waggoner, T. B. Bartnikas, J. D. Gitlin, *Neurobiol. Dis.* **1999**, *6*, 221.
- [10] J. Giersz, M. Bartosiak, K. Jankowski, *Talanta* **2017**, *167*, 279.
- [11] G. Özzeybek, S. Erarpat, D. S. Chormey, M. Firat, Ç. Büyükrınar, F. Turak, *Microchem. J.* **2017**, *132*, 406.
- [12] D. Grujicic, B. Pesic, *Electrochim. Acta* **2002**, *47*, 2901.
- [13] Y. Q. Zhang, G. Wang, J. P. Zhang, *Sens. Actuators B* **2014**, *200*, 259.
- [14] L. H. Liu, A. X. Wang, G. Wang, J. X. Li, Y. H. Zhou, *Sens. Actuators B* **2015**, *215*, 388.
- [15] F. Abebe, T. Sutton, P. Perkins, R. Shaw, *Luminescence* **2018**, *33*, 1.
- [16] Shaily, A. Kumar, I. Parveen, N. Ahmed, *Luminescence* **2018**, *33*, 713.
- [17] L. Zhu, C. Gu, Y. He, G. Wang, *J. Lunim.* **2014**, *153*, 439.
- [18] L. Wang, X. Gong, Q. J. Bing, G. Wang, *Microchem. J.* **2018**, *142*, 279.

- [19] K. Wechakorn, S. Prabbai, K. Suksen, P. Kanjanasirirat, Y. Pewkliang, S. Borwornpiny, P. Kongsaree, *Luminescence* **2018**, *33*, 64.
- [20] L. J. Tang, P. Zhou, K. L. Zhong, S. H. Hou, *Sens. Actuators B* **2013**, *182*, 439.
- [21] L. L. Li, H. Li, G. Liu, S. Z. Pu, *Luminescence* **2017**, *32*, 1473.
- [22] I. M. El-Sewify, M. A. Shenashen, A. Shahat, M. M. Selim, M. M. H. Khalil, *S.A. Microchem. J.* **2018**, *139*, 24.
- [23] Y. He, J. Yin, G. Wang, *Chem. Heterocycl. Compd.* **2018**, *54*, 146.
- [24] D. H. Li, A. Munitywali, G. Wang, M. D. Zhang, S. X. Xing, *Dyes Pigm.* **2015**, *117*, 92.
- [25] S. Q. Wang, Y. L. Si, C. Y. Tong, G. Wang, B. Qi, G. C. Yang, *Opt. Mater.* **2013**, *35*, 1504.
- [26] Y. He, G. Wang, M. X. Wang, *J. Mol. Struct.* **2016**, *1116*, 109.
- [27] Q. J. Bing, L. Wang, D. L. Li, G. Wang, *Spectrochim Acta a* **2018**, *202*, 305.
- [28] V. A. Bren, I. E. Tolpygin, K. S. Tikhomirova, O. S. Popova, Z. V. Bren, Y. V. Revinskii, *A.D. Chem. Heterocycl. Compd.* **2015**, *50*, 1665.
- [29] S. Maria, P. Claudio, *Coord. Chem. Rev.* **2016**, *318*, 16.
- [30] J. H. Chang, Y. M. Choi, Y. K. Shin, *Bull. Korean. Chem. Soc.* **2001**, *22*, 527.
- [31] M. G. Choi, S. Y. Cha, H. K. Lee, H. L. Jeon, S. K. Chang, *Chem. Commun.* **2009**, *47*, 7390.
- [32] L. Zhang, X. D. Lou, Y. Yu, J. G. Qin, Z. Li, *Macromolecules* **2011**, *44*, 5186.
- [33] M. Silvia, M. Stefano, S. Maria, P. Claudio, *Eur. J. Inorg. Chem.* **2015**, *13*, 3900.
- [34] Y. K. Tsui, S. Devaraj, Y. P. Yen, *Sens. Actuators B* **2012**, *161*, 510.
- [35] J. W. Liu, Y. Lu, *J. Am. Chem. Soc.* **2007**, *129*, 9838.
- [36] C. Y. Li, X. B. Zhang, Z. Jin, R. Han, G. L. Shen, R. Q. Yu, *Anal. Chim. Acta* **2006**, *580*, 143.
- [37] R. Nudelman, O. Ardon, Y. Hadar, Y. N. Chen, J. Libman, A. Shanzer, *J. Med. Chem.* **1998**, *41*, 1671.
- [38] M. J. Frisch, G. W. Trucks, H. B. Schlegel, G. E. Scuseria, M. A. Robb, J. R. Cheeseman, G. Scalmani, V. Barone, B. Mennucci, G. A. Petersson, H. Nakatsuji, M. Caricato, X. Li, H. P. Hratchian, A. F. Izmaylov, J. Bloino, G. Zheng, J. L. Sonnenberg, M. Hada, M. Ehara, K. Toyota, R. Fukuda, J. Hasegawa, M. Ishida, T. Nakajima, Y. Honda, O. Kitao, H. Nakai, T. Vreven, J. Montgomery, J. A., J. E. Peralta, F. Ogliaro, M. Bearpark, J. J. Heyd, E. Brothers, K. N. Kudin, V. N. Staroverov, R. Kobayashi, J. Normand, K. Raghavachari, A. Rendell, J. C. Burant, S. S. Iyengar, J. Tomasi, M. Cossi, N. Rega, N. J. Millam, M. Klene, J. E. Knox, J. B. Cross, V. Bakken, C. Adamo, J. Jaramillo, R. Gomperts, R. E. Stratmann, O. Yazyev, A. J. Austin, R. Cammi, C. Pomelli, J. W. Ochterski, R. L. Martin, K. Morokuma, V. G. Zakrzewski, G. A. Voth, P. Salvador, J. J. Dannenberg, S. Dapprich, A. D. Daniels, Ö. Farkas, J. B. Foresman, J. V. Ortiz, J. Cioslowski and D. J. Gaussian 09. revision D.01, Gaussian Inc, Wallingford **2013**.
- [39] P. Marimuthu, A. Ramu, *Sens. Actuators B* **2018**, *266*, 384.
- [40] S. K. Sahoo, D. Sharma, A. Moirangthem, K. Aman, B. Anupam, *J. Lumin.* **2016**, *172*, 297.

SUPPORTING INFORMATION

Additional supporting information may be found online in the Supporting Information section at the end of the article.

How to cite this article: He Y, Bing Q, Wei Y, Zhang H, Wang G. A new benzimidazole-based selective and sensitive 'on-off' fluorescence chemosensor for Cu²⁺ ions and application in cellular bioimaging. *Luminescence*. 2019;1-9. <https://doi.org/10.1002/bio.3586>